Optics Letters

175 W average power from a single-core rod fiber-based chirped-pulse-amplification system

Martin E. V. Pedersen,* Mette M. Johansen, Anders S. Olesen, Mattia Michieletto, Maxim Gaponenko, and Martin D. Maack

NKT Photonics A/S, Blokken 84, 3460 Birkerød, Denmark
**Corresponding author: mpe@nktphotonics.com*

Received 27 July 2022; revised 9 September 2022; accepted 12 September 2022; posted 12 September 2022; published 28 September 2022

We report on a fiber-based chirped-pulse-amplification laser system with bulk transmission grating compression to a pulse duration of 357 fs, average power of 175 W, and pulse energy of 233 μJ. The compressed pulse train has a beam quality factor M^2 of 1.21. The power amplifier is based on a state-of-the-art single-mode photonic crystal rod-type ytterbium-doped fiber operating at 248 W of average power and a repetition rate of 750 kHz. The long-term stability of the laser system has been tested continuously for more than 4000 hours and shows no sign of transverse mode instability.

https://doi.org/10.1364/OL.471631

Fiber-based amplifiers have attracted much attention from both academia and industry, due to the large surface to volume ratio offered by optical fibers and the resulting advantages with respect to thermal management, pushing the boundaries for average power scaling, while at the same time maintaining near diffraction limited beam quality. However, optical nonlinearity becomes an increasing problem for scaling power, due to the long interaction length and relatively small effective area offered by traditional gain fibers. The threshold for nonlinear effects can be increased by increasing the effective area of the guided mode in the active fiber and by increasing pump absorption, thereby decreasing the effective length of the amplifier [1,2]. Another way to counter nonlinear effects is to lower the intensity in the fiber by using a chirped-pulse-amplification (CPA) scheme, based on stretching the pulse in time before the amplification stage followed by an external temporal compression [3]. Further power scaling with near diffraction limited output may be achieved through coherent beam combination of a multi-channel amplification system [4] or in a multi-core fiber configuration [5]. Another limitation for fiber based amplifiers, including rod-fiber amplifiers, is the onset of transverse mode instability (TMI) limiting the average power that can be extracted while maintaining stable operation. If the TMI level in the amplifier becomes significant, it will impact the beam quality and stability, as the output mode will contain a significant amount of higher-order-mode content and reduce the quality of the laser output. The onset of TMI is, among other things, related to the heat load per unit length of the fiber and the finite suppression of higher-order modes (HOMs) [6–10]. Ways to mitigate TMI therefore include means to reduce the heat load as well as fiber designs ensuring strong suppression of HOMs.

In this paper, we focus on power scaling in single-channel amplifiers and take advantage of both the CPA scheme as well as the large effective area of ytterbium-doped rod-fiber amplifiers with TMI thresholds well-above 250 W of average power. Individual reports of single-channel fiber-based CPA systems have previously been published demonstrating average power in excess of 100 W [11], pulse duration less than 400 fs [12,13], or pulse energy above 150 μJ [14]. It is desirable to combine high pulse energy levels with repetition rates approaching MHz level. In this paper, we demonstrate a single-channel CPA system with 233 μJ of pulse energy operating at a repetition rate of 750 kHz, which has not previously been achieved to the best of our knowledge. It is achieved by having an average power of 175 W, a pulse duration of 357 fs, and a beam quality factor M^2 of 1.21 after re-compression.

A schematic of the full CPA system is shown in Fig. 1 comprising a front end (section 1), a power amplifier based on rod-fiber amplifiers (section 2), and a compressor (section 3). Following the compressor, the output is analyzed in terms of power, temporal, spectral, and spatial characteristics (section 4). The front end comprises a mode-locked seed laser providing a pulse train of 170 fs pulses at a center wavelength of 1029 nm, and at a repetition rate of 40 MHz. The pulses from the seed laser are temporally stretched in a dual-stretcher fiber Bragg grating based configuration with mid-stage amplification (Amp 1) followed by an acousto-optic modulator (AOM) reducing the pulse repetition rate down to 750 kHz, and two additional fiber amplifiers labeled Amp 2 and Amp 3. The repetition rate is lowered to increase the pulse energy. Amp 1 and Amp 2 are both standard 6-μm core pumped step-index single-mode fiber based amplifiers, whereas Amp 3 is based on a double-clad ytterbium-doped fiber (DC-135/14-PM-Yb from NKT Photonics). The fiber front-end section delivers 500 mW of output power with a full width half maximum (FWHM) pulse duration of 1.5 ns. The output from the front end is free-spaced coupled to the first rod-fiber amplifier (Amp 4) which delivers 25 W of output power coupled to the second rod-fiber amplifier (Amp 5), where the signal is further amplified to 248 W corresponding to a pulse energy of 333 μJ and a peak power of 216 kW. Amp 4 is based on a

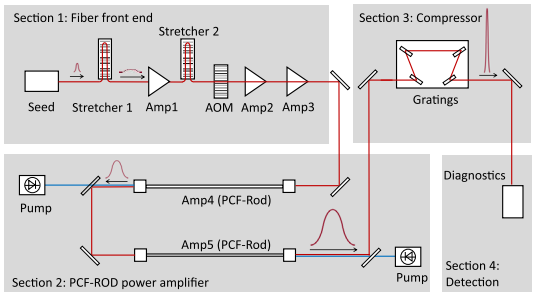

Fig. 1. Schematic setup of the CPA system using the rod amplifiers with the bulk compressor for temporal re-compression of the optical pulse.

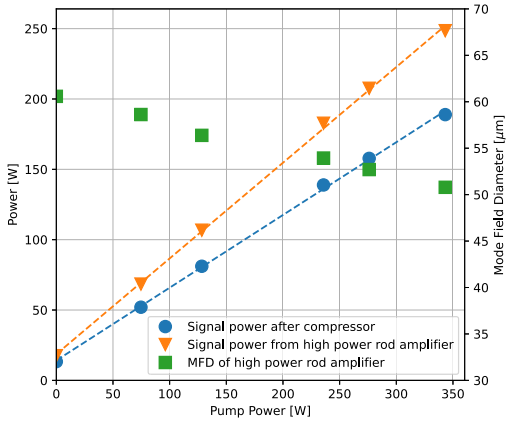

Fig. 2. Signal power after the compressor together with the MFD and the power output of the second rod-fiber amplifier are shown as a function of pump power. The MFD is measured by taping the beam right after the collimated output of the amplifier. The end-facet of the rod-fiber is imaged to a camera with a microscope setup.

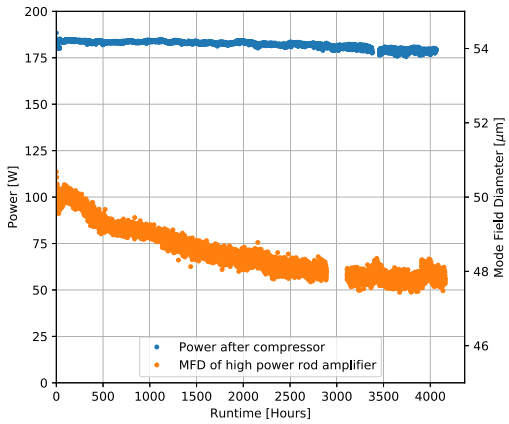

Fig. 3. Signal power evolution after the compressor and MFD of the second rod-fiber amplifier is shown as a function of run-time. The gap in the data is due to data logging failure. Stop and start effects in the power measurement have been removed for clarity.

standard commercially available *aeroGAIN-ROD* (aeroGAIN-ROD-PM85 from NKT Photonics), while the rod-fiber used in Amp 5 is an improved version of the *aeroGAIN-ROD* developed to suppress the TMI onset allowing to scale power. Both rod-fibers used on Amp 4 and Amp 5 have a core size of 85 μm surrounded by a photonic crystal cladding structure and a 260 μm pump guide. The passive mode-field diameter (MFD) of both rod-fibers without the presence of heat load is 60 μm–65 μm at 1030 nm. All amplifiers in both the front-end and power amplifier section are backward pumped and, with the exception of Amp 1, there is an optical isolator following all amplification stages. The pump lasers for the two rod-fiber amplifier stages are volume Bragg grating stabilized with an operation wavelength of 976 nm. (Pump lasers for Amp 4 and Amp 5: *e18.130.0976200* from nLight and *D4F2Q22-976.0,6-400C-IS45.11* from DILAS now Coherent.) The output of the power amplifier is passed through two twofold table-top bulk optical compressors, before the laser output is characterized. The bulk transmission gratings in the compressor yields a overall transmission of the two twofold compressors of ≈ 80%. In Fig. 2 the average signal power measured after the compressor is shown along with the average signal power and MFD from the output of Amp 5, all as a function of the pump power in Amp 5. The pump to signal slope efficiency for the signal out of the compressor is 0.52. For the power output of Amp 5 before the transmission through the compressor, the slope efficiency is 0.68. As the *aeroGAIN-ROD* is a large core single-mode fiber, the numerical aperture is correspondingly small, which in turn makes the NA susceptible to thermally driven index changes, which for silica are of the order of $\approx 1 \times 10^{-5}$ K^{-1} [15]. It is the heating of the fiber core which, through the effect of thermal lensing, causes the MFD of the fiber to change from ≈ 60 μm to ≈ 50 μm as the signal power is ramped from zero to 248 W.

The long-term stability of the full CPA system including front-end, power amplifier, and compressor has been tested continuously for more than 4000 hours. The main motivation for a long-term test of this duration is that TMI is a function of the accumulated photo-darkening (PD) over time. PD causes an increasing amount of heat to be deposited in the fiber, in turn leading to a reduction of the TMI threshold [16,17]. In [16], the heat-load contribution from the PD process is shown to be more than 50% of the total heat load and this contribution cannot be expected to be observed from only a short-term test.

The evolution of the signal output power measured after the compressor and the MFD at the output of the rod-fiber in Amp 5 as a function of run-time are shown in Fig. 3.

Over the full duration of the long-term test, the decay in measured output power from the compressor is approximately 10 W comprised by a 4 W decay observed during the initial 30 hours of the test followed by a gradual decay of 6 W over the following 4000 hours corresponding to a rate of ≈ 0.8% per 1000 hours.

Over the course of the long-term test, a reduction in MFD of 2 μm, corresponding to a relative change of 4%, is observed. The rate of change appears to decrease over time and during the last more than 1000 hours of the test, the variations in MFD are less than the measurement uncertainty indicating a saturation in the MFD value. The change in MFD is attributed to a gradual change of refractive index of the fiber core, which in turn is caused directly by the PD-induced index changes as well as a slight increase in thermal lensing related to the PD-induced heat load.

In Fig. 4, data of the auto-correlation trace measured after the compressor along with the associated $sech^2$ fit, the output wavelength spectrum, and an insert of the intensity profile of the rod-fiber in Amp 5 are shown for run-times of 0 hours,

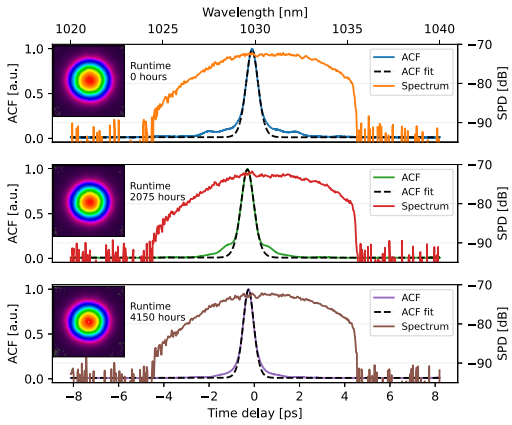

Fig. 4. Auto-correlation and spectrum measurement for different run-times: 0 hours; 2075 hours; and 4150 hours from top to bottom, respectively. The insets on the left show the mode profile of the second rod amplifier. The size of the sidebands in the auto-correlation does not change significantly in the course of the long-term test.

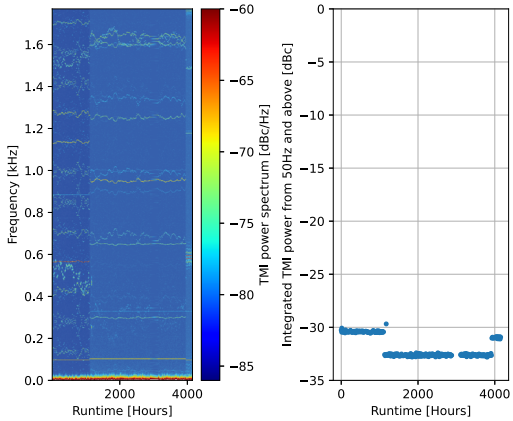

Fig. 5. Spectrogram of the (a) TMI and the (b) integrated TMI power. To remove the contribution from the mechanical movements, the lower limit of the integrated TMI power is 50 Hz. The detail TMI spectrogram shown on the left requires a high DPI level, which might not be available in a printout and the reader is referred to the online version.

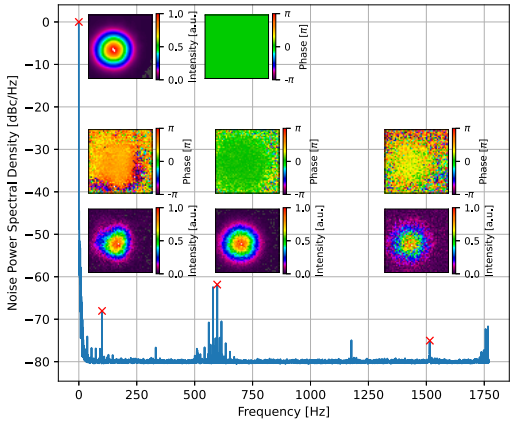

Fig. 6. TMI power spectral density at the end of the long-term test. The intensity and phase of the spatially reconstructed modes are shown for the peaks with a red cross. All peaks have a fundamental mode signature in the intensity and phase, hence a result of modulation intensity.

2075 hours, and 4150 hours. The auto-correlation traces have small-intensity sidebands, caused by a nonlinear phase shift accumulated during the amplification process, and show fair agreement with the sech^2 fit indicating a good re-compression of the pulse. The auto-correlation traces were measured approximately one time per hour during the full long-term test. The CPA system is built in a free-space table-top configuration, and the pulse duration is sensitive to changes in ambient conditions such as lab temperature. Despite this, the measured pulse duration is below 400 fs for the majority of the run-time and shows a median value of 357 fs. The rod amplifiers are not subjected to the same change in the ambient temperature as the rod modules are water cooled and kept at a constant temperature of 25°C.

Similar to the auto-correlation, the output spectrum was also recorded approximately once per hour. The average 3 dB (FWHM) and 10 dB bandwidth of the spectrum after the compressor is 5.5 nm and 9.6 nm, respectively. The final 3 dB bandwidth of the spectrum is a result of the transmission and gain shaping of the initial spectrum through the different stages of the CPA system. The 3 dB bandwidths of the seed laser, front-end, amp 4, and amp 5 are 6.8 nm, 6.7 nm, 6.4 nm, and 5.8 nm, respectively. The spectrum remains stable throughout the duration of the long-term test. It is noted that the spectrum is abruptly cut on the long-wavelength side due to a spatial beam cutoff on compressor gratings. The spectrum show intensity ripples, indicating a contribution of nonlinear phase-shift, which may impact the re-compression level. The tests performed at the repetition rates below 750 kHz confirmed that increased pulse energy causes larger intensity ripples in the pulse spectrum and results in increased sidebands observed in auto-correlation traces. Using the measured output spectrum of the compressed pulse and assuming zero phase, then the transform-limited pulse duration is calculated to 330 fs.

The M^2-values of the output beam after the compressor are measured point-wise during the long-term test and remain constant with small fluctuations. The average values from 96 measurements of the M^2-values are $M_x^2 = 1.21$, $M_y^2 = 1.17$, Astigmatism = 0.07, and Asymmetry = 1.15. In the insets of Fig. 4, the mode profiles of the output beam from the Amp 5 are shown. The beam has a Gaussian-like spatial profile with $M_x^2 = 1.04$, $M_y^2 = 1.04$, Astigmatism = 0.02, and Asymmetry = 1.03. For this high power CPA system, the high beam quality is ensured by the rod-fiber amplifier.

The evolution of the TMI content characterized at the output Amp 5 throughout the full duration of the long-term test is shown in Fig. 5. The TMI dynamics are investigated and analyzed with a fast camera using the *ST-method* [18], providing in-depth details about TMI dynamics of the amplifier.

Most of the peaks in the spectrogram change frequency during the long-term test. A detailed investigation of these peaks, using the *ST-method*, reveals that the majority of the peaks are associated with intensity modulation. Examples of the intensity modulation peaks are shown in Fig. 6. The repetition rate of the laser output is much higher than the sampling rate of the camera, hence the under-sampled laser repetition rate can be mapped to wrong frequencies. The discrete lines in time in Fig. 5 are where the overall dynamics changes are associated with the system being turned off and on with changes in the integration

time of the camera. The integrated TMI level remains negligible throughout the long-term test with a maximum value less than −29 dBc including also the intensity modulation peaks. An important fact is that even though there is some parasitic PD in the long-term test, as seen in Fig. 3, the additional heat-load does not impact the TMI signal, which validates the increased TMI resistance of the improved *aeroGAIN-ROD*. The previous generation of the *aeroGAIN-ROD* was tested in the setup and showed a TMI signal stronger than −15 dBc under the same test conditions. This is in line with other reported TMI values at the same power level for the *aeroGAIN-ROD* and other types of rod amplifier fibers, which show a clear TMI signal [17,19,20]. The low TMI signal of the improved *aeroGAIN-ROD* demonstrates that this power-level is stable for long-term operation and that the CPA system is not TMI limited.

In conclusion, we have demonstrated a single-core rod fiber-based CPA system delivering 357 fs pulses at 1030 nm with a repetition rate of 750 kHz, 175 W average power, 233 μJ pulse energy, and an M^2 of 1.21. We have shown that the long-term effects on a state-of-the-art single-mode photonic crystal rod-type ytterbium-doped fiber do not give rise to any increase of TMI due to photo-darkening, which makes it possible to operate the amplifier at 248 W average power for more than 4000 hours free of TMI. This demonstrates that large core photonic crystal fibers are a suitable technology to realize laser systems with near diffraction-limited output beam quality delivering ultrashort pulses with energy of hundreds of μJ at near-MHz repetition rates. Development in the thermal management and scaling of fiber core size will provide a route for further power scaling.

Disclosures. Martin E. V. Pedersen, NKT Photonics A/S (E); Mette M. Johansen, NKT Photonics A/S (E); Anders S. Olesen, NKT Photonics A/S (E); Mattia Michieletto, NKT Photonics A/S (E); Maxim Gaponenko, NKT Photonics A/S (E); Martin D. Maack, NKT Photonics A/S (E).

Data availability. Data underlying the results presented in this paper are not publicly available at this time but may be obtained from the authors upon reasonable request.

REFERENCES

1. D. J. Richardson, J. Nilsson, and W. A. Clarkson, J. Opt. Soc. Am. B **27**, B63 (2010).
2. T. T. Alkeskjold, M. Laurila, L. Scolari, and J. Broeng, Opt. Express **19**, 7398 (2011).
3. D. Strickland and G. Mourou, Opt. Commun. **55**, 447 (1985).
4. M. Müller, C. Aleshire, A. Klenke, E. Haddad, F. Légaré, A. Tünnermann, and J. Limpert, Opt. Lett. **45**, 3083 (2020).
5. C. Aleshire, A. Steinkopff, A. Klenke, C. Jáuregui, S. Kuhn, J. Nold, N. Haarlammert, T. Schreiber, and J. Limpert, Opt. Lett. **47**, 1725 (2022).
6. T. Eidam, C. Wirth, C. Jauregui, F. Stutzki, F. Jansen, H.-J. Otto, O. Schmidt, T. Schreiber, J. Limpert, and A. Tünnermann, Opt. Express **19**, 13218 (2011).
7. H.-J. Otto, F. Stutzki, F. Jansen, T. Eidam, C. Jauregui, J. Limpert, and A. Tünnermann, Opt. Express **20**, 15710 (2012).
8. M. M. Johansen, M. Laurila, M. D. Maack, D. Noordegraaf, C. Jakobsen, T. T. Alkeskjold, and J. Laegsgaard, Opt. Express **21**, 21847 (2013).
9. K. R. Hansen, T. T. Alkeskjold, J. Broeng, and J. Laegsgaard, Opt. Express **21**, 1944 (2013).
10. F. Kong, J. Xue, R. H. Stolen, and L. Dong, Optica **3**, 975 (2016).
11. M. Wang, P. Li, S. Li, Y. Xu, and C. Yao, Optik **253**, 168597 (2022).
12. K. Kim, X. Peng, W. Lee, S. Gee, M. Mielke, T. Luo, L. Pan, Q. Wang, and S. Jiang, Opt. Express **23**, 4766 (2015).
13. X. Li, M. A. R. Reber, C. Corder, Y. Chen, P. Zhao, and T. K. Allison, Rev. Sci. Instrum. **87**, 093114 (2016).
14. F. Li, W. Zhao, Y. Wang, N. Wang, Q. Li, Y. Yang, and W. Wen, Opt. Laser Technol. **147**, 107684 (2022).
15. P. Dragic, M. Cavillon, and J. Ballato, Opt. Mater. Express **7**, 3654 (2017).
16. C. Jauregui, H.-J. Otto, F. Stutzki, J. Limpert, and A. Tünnermann, Opt. Express **23**, 20203 (2015).
17. M. M. Johansen, M. Michieletto, T. Kristensen, T. T. Alkeskjold, and J. Laegsgaard, Proc. SPIE **9728**, 97280I (2016).
18. S. L. Christensen, M. M. Johansen, M. Michieletto, M. Triches, M. D. Maack, and J. Laegsgaard, Opt. Express **28**, 26690 (2020).
19. F. Jansen, F. Stutzki, H.-J. Otto, T. Eidam, A. Liem, C. Jauregui, J. Limpert, and A. Tünnermann, Opt. Express **20**, 3997 (2012).
20. M.-A. Malleville, A. Benoît, R. Dauliat, B. Leconte, D. Darwich, R. du Jeu, R. Jamier, A. Schwuchow, K. Schuster, and P. Roy, Proc. SPIE **10512**, 1051206(2018).